VIII International Conference on Fracture Mechanics of Concrete and Concrete Structures
FraMCoS-8
J.G.M. Van Mier, G. Ruiz, C. Andrade, R.C. Yu and X.X. Zhang (Eds)

MODELLING OF CHLORIDE TRANSPORT IN NON-SATURATED CONCRETE. FROM MICROSCALE TO MACROSCALE

Michiel M.C. Fenaux*, Encarnación Reyes*, Amparo Moragues* and Jaime C. Gálvez*

*Universidad Politécnica de Madrid (UPM)
ETS de Ingenieros de Caminos, Canales y Puertos
Calle Profesor Aranguren s/n, 28004 Madrid, Spain
e-mail: mfenaux@caminos.upm.es, www.upm.es
e-mail: ereyes@caminos.upm.es, www.upm.es
e-mail: amoragues@caminos.upm.es, www.upm.es
e-mail: jcgalvez@caminos.upm.es, www.upm.es

Key words: Chloride Transport, Pore Solution Transport, Modelling, Equivalent Pore, Finite Elements

Abstract. This work shows the chloride transport equations at the macroscopic scale in non-saturated concrete. The equations involve diffusion, migration, capillary suction, chloride combination and precipitation mechanisms. The material is assumed to be infinitely rigid, though the porosity can change under influence of chloride binding and precipitation. The involved microscopic and macroscopic properties of the materials are measured by standardized methods. The variables which must be imposed on the boundaries are temperature, relative humidity and chloride concentration. The output data of the model are the free, bound, precipitated and total chloride ion concentrations, as well as the pore solution content and the porosity. The proposed equations are solved by means of the finite element method (FEM) implemented in MATLAB (classical Galerkin formulation and the streamline upwind Petrov-Galerkin (SUPG) method to avoid spatial instabilities for advection dominated flows).

1 INTRODUCTION

Chloride penetration into reinforced concrete causes corrosion of the reinforcement bars. The expansion of the resulting corrosion products (iron oxides) can induce mechanical stress which can lead to formation of cracks. Therefore, it is important to predict the time the chloride ions need to reach the reinforcement bars.

Basic models of chloride transport are based on a linear diffusion equation [1, 2]:

$$\frac{\partial C}{\partial t} = D_e \boldsymbol{\nabla}.\left(\boldsymbol{\nabla} C\right) \qquad (1)$$

where C is the free chloride concentration (kg/m^3 of solution) and D_e the so-called effective diffusion coefficient (m^2/s). Equation 1 is only valid for fully saturated and non-reactive concrete. To distinguish between free and total chloride ion diffusion, Saetta et al. [3] used two different kinds of diffusion coefficients, namely the effective diffusion coefficient D_e and the apparent diffusion coefficient D_a, both expressed in m^2/s. Denoting the total chloride concentration as C_t and the free chloride concentration as C_f, both expressed in kg/m^3 of concrete. Then, the diffusion equations are given by:

$$\frac{\partial C_t}{\partial t} = \boldsymbol{\nabla}.\left(D_e \boldsymbol{\nabla} C_f\right) \qquad (2)$$

$$\frac{\partial C_t}{\partial t} = \boldsymbol{\nabla}.\left(D_a \boldsymbol{\nabla} C_t\right) \qquad (3)$$

Coussy and Ulm [4] used a diffusion-reaction model contemplating the chloride binding, based on D_e:

$$\frac{\partial(\phi C)}{\partial t} + \frac{\partial([1-\phi]C_b)}{\partial t} = \boldsymbol{\nabla}.\left(\phi D_e \boldsymbol{\nabla} C\right) \quad (4)$$

where ϕ is the porosity and $(1-\phi)$ corresponds to the relative volume of solid material. A value of $2.3\times10^{-12}m^2/s$ was adopted for ϕD_e. Equation 4 is valid for saturated concrete ($\phi_l = \phi$). Samson et al. [5] derived the mass transport equations using the homogenization technique and obtained the following chloride ion transport model for fully saturated and non-reactive concrete:

$$\frac{\partial C}{\partial t} = \boldsymbol{\nabla}.\left(D_e \boldsymbol{\nabla} C - \frac{F D_e}{RT} C \boldsymbol{\nabla}\Phi\right) \quad (5)$$

where R and F are the gas and the Faraday constants, respectively, and Φ the electric potential.

In this paper, the macroscopic transport equations for chloride ions in unsaturated hardened concrete are derived from the microscopic equations. This is carried out by comparing the porous network with one single *equivalent pore* whose properties are the same as the properties of the real porous network. The resulting system of differential equations is then solved by means of the finite element method (FEM) on an unstructured *2D* mesh of triangular elements. Several standard test methods were employed to characterize the intrinsic properties of the studied materials.

2 GENERAL CONSIDERATIONS

Different types of chloride concentrations are used in this work. The free chloride concentration C expressed in kg/m^3 or g/l of pore solution, and the free chloride concentration C_f expressed in kg/m^3 of concrete. Those quantities are related to each other by means of the evaporable water content ϕ_l, expressed in m^3/m^3 of concrete:

$$C_f = \phi_l C \quad (6)$$

Furthermore, the bound and the total chloride concentrations are denoted by C_b and C_t, respectively, and both are expressed in kg/m^3 of concrete. The total chloride concentration can be expressed as a function of the free and bound chloride concentrations as follows:

$$C_t = C_f + C_b = \phi_l C + C_b \quad (7)$$

3 MASS FLUXES AT THE MICROSCALE LEVEL

In the absence of advective flows and chloride binding, the flux of dissolved ions in a fluid is generally described as a function of the gradient of an electrochemical potential. The electrochemical potential can be interpreted as the mechanical work performed by moving one mole from a reference state to another state defined by its chemical concentration and electrical potential. The mathematical definition for species i is [6]:

$$\overline{\mu}_i = \mu_i^0 + RT\ln(\gamma_i C_i) + z_i F\Phi \quad (8)$$

where the subscript i refers to the ion species, $\overline{\mu}_i$ is the electrochemical potential (J/mol), μ_i is the chemical potential at a reference state (J/mol), z_i the valency of ion i ($z = -1$ for Cl^-), and γ_i is the chemical activity coefficient. The gradient of the electrochemical potential reads:

$$\begin{aligned}\boldsymbol{\nabla}\overline{\mu}_i &= D_i \boldsymbol{\nabla} C_i + \frac{F D_i}{RT} z_i C_i \boldsymbol{\nabla}\Phi \\ &+ \frac{1}{T}\ln(\gamma_i C_i) D_i C_i \boldsymbol{\nabla} T \end{aligned} \quad (9)$$

where D_i is the diffusion coefficient of species i. Samson et al. [7] showed that the effect of chemical activity on chloride penetration is negligible. Therefore, the last term on the right hand side of Equation 9 can be ignored. While temperature has a high influence on chloride penetration, the temperature gradient does not [8]. Denoting the diffusion coefficient in water of species i by D_i and multiplying Equation 9 by $D_i C_i/RT$, yields:

$$\frac{D_i C_i}{RT}\boldsymbol{\nabla}\overline{\mu}_i = D_i \boldsymbol{\nabla} C_i + \frac{F D_i}{RT} z_i C_i \boldsymbol{\nabla}\Phi \quad (10)$$

For chloride ions, $D_i = D_{Cl}$, $C_i = C$ and $z_i = -1$, the diffusive and electric fluxes at

the microscopic scale are deduced directly from Equation 10:

$$\boldsymbol{J}_D^{\mu} = -D_{Cl}\boldsymbol{\nabla}C \quad (11)$$

$$\boldsymbol{J}_P^{\mu} = \frac{FD_{Cl}}{RT}C\boldsymbol{\nabla}\Phi \quad (12)$$

The advective flux, due to capillary suction, is modelled at the macroscopic scale by means of Darcy's law.

4 MASS FLUXES AT THE MACROSCALE LEVEL

4.1 The diffusive flux

A general expression for the diffusive flux at the macroscopic scale is:

$$\boldsymbol{J}_D = -D\boldsymbol{\nabla}C \quad (13)$$

where D is the diffusion coefficient (m^2/s) determined below.

Consider a single cylindrical pore, completely saturated with an aqueous *NaCl* solution (the pore solution). The total amount of chloride ions, expressed in kilograms that crosses a transverse section a of the pore per second, is:

$$a\boldsymbol{J}_{Cl}^{\mu} = -aD_{Cl}\boldsymbol{\nabla}C \quad (14)$$

where $\boldsymbol{J}_{Cl}^{\mu}$ is the flux of chlorides due to diffusion at the pore scale. It is worth noting that Equation 14 holds for any transverse section and not only for circular sections, as long as it is constant along the longitudinal axis of the pore. Next, a partially saturated infinitesimal volume of concrete is considered (Figure 1). The cross section dA of the volume is taken to be small enough so that the concentrations in each pore (for a given depth) can be considered equal. dx is the thickness of the volume.

The volume is partially saturated. The equivalent pore is a fully saturated cylindrical pore of length dx, where the radius is such that the volume of the equivalent pore equals the sum of the volumes of the pores containing water.

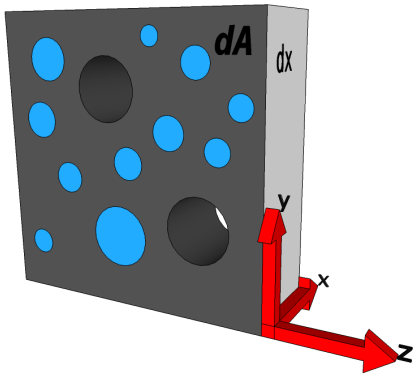

Figure 1: Partially saturated infinitesimal volume of concrete.

Denoting the cross section of the equivalent pore by da_w, the total amount of chloride ions expressed in kilograms that crosses a transverse section da_w of the pore per second is:

$$da_w\boldsymbol{J}_{Cl}^{eq} = -da_wD_{Cl}\boldsymbol{\nabla}C \quad (15)$$

where $\boldsymbol{J}_{Cl}^{eq}$ is the diffusive flux of chloride ions in the equivalent pore, which is a macroscopic quantity. Until now, the pores have been assumed to be straight and cylindrical. However, real pores are usually neither cylindrical, nor continuous or parallel one to another. This implies that the gradient of the concentration is no longer the same in the real pores as in the equivalent pore. Indeed, the latter is much more important in magnitude. Therefore, the flux in the equivalent pore must be corrected, which is done by means of the tortuosity-connectivity parameter τ. The shape of the equivalent pore remains the same, though its diffusive properties change. The total amount of chloride ions expressed in kilograms that crosses a transverse section da_w of the modified equivalent pore per second is now:

$$da_w\boldsymbol{J}_{Cl}^{eq} = -da_w\tau D_{Cl}\boldsymbol{\nabla}C \quad (16)$$

This amount of chlorides coincides with the amount of chlorides which pass the cross section dA of the infinitesimal volume per second, and can therefore be expressed as:

$$dA\boldsymbol{J}_D = -dAD\boldsymbol{\nabla}C \quad (17)$$

Multiplying Equations 16 and 17 by dx, and setting them equal to each other, yields:

$$dAdxD\boldsymbol{\nabla}C = da_wdx\tau D_{Cl}\boldsymbol{\nabla}C \quad (18)$$

where $dAdx$ is the volume of the continuum $d\Omega$ and $da_w dx$ is the volume of the equivalent pore $d\Omega_w$. The diffusion coefficient D is deduced directly from Equation 18:

$$D = \frac{d\Omega_w}{d\Omega}\tau D_{Cl} \quad (19)$$

where $d\Omega_w/d\Omega$ is the water content ϕ_l expressed in m^3/m^3 of concrete. The diffusive flux at the macroscopic scale reads:

$$\boldsymbol{J}_D = -\tau\phi_l D_{Cl}\boldsymbol{\nabla} C \quad (20)$$

The effective diffusion coefficient D_e can now be written as $D_e = \tau D_{Cl}$, and is an intrinsic parameter of the material. Indeed, it solely depends on the diffusion coefficient of chlorides in water and on the properties of the material, τ.

4.2 The electric flux

The traditional expression for the electric flux of chloride ions is:

$$\boldsymbol{J}_P = -P\boldsymbol{\nabla}\Phi \quad (21)$$

where P is the proportionality coefficient. Following the same procedure as for the diffusive flux, starting from Equation 12, the coefficient P can be determined:

$$P = -\frac{\tau F}{RT}D_{Cl}\phi_l C \quad (22)$$

The electric potential Φ can be calculated by means of the Poisson equation for electrostatics. However, since the potential is induced by the diffusion of chlorides (and other ions), the electric flux can be expressed as a diffusive flux, which is further explored below.

When *NaCl* is dissolved in water, the sodium and chloride ions are separated according to the following dissolution reaction:

$$NaCl(s) \longrightarrow Na^+(aq) + Cl^-(aq) \quad (23)$$

For the sake of simplicity, the Na^+ and Cl^- ions are assumed to come from dissolved molecules of *NaCl* solely. These ions are transported by diffusion, by the electric flux and by advection (capillary suction). The total flux of each species reads:

$$\begin{aligned} \boldsymbol{J}_{Na} &= -\hat{D}_{Na}\boldsymbol{\nabla} C_{Na} - P_{Na}\boldsymbol{\nabla}\Phi \\ &+ \boldsymbol{u}C_{Na} \quad (24) \\ \boldsymbol{J}_{Cl} &= -\hat{D}_{Cl}\boldsymbol{\nabla} C_{Cl} - P_{Cl}\boldsymbol{\nabla}\Phi \\ &+ \boldsymbol{u}C_{Cl} \quad (25) \end{aligned}$$

where $\boldsymbol{u}$ is the advection velocity and the subscripts *Na* and *Cl* refer to the ion species. The other coefficients are given below:

$$\hat{D}_i = \tau\phi_l D_i \qquad P_i = \tau\frac{z_i F}{RT}D_i\phi_l C_i \quad (26)$$

where i refers to the species, Na^+ or Cl^-. The current density associated to the ionic fluxes is given by:

$$I = \frac{z_{Na}F}{m_{Na}}\boldsymbol{J}_{Na} + \frac{z_{Cl}F}{m_{Cl}}\boldsymbol{J}_{Cl} \quad (27)$$

where I is the current density (A/m^2) and m_i is the molar mass of species i (kg/mol). Substitution of Equations 24-25 into Equation 27 yields:

$$\begin{aligned} I &= F\left(\left[\frac{\hat{D}_{Cl}}{m_{Cl}}\boldsymbol{\nabla} C_{Cl} - \frac{\hat{D}_{Na}}{m_{Na}}\boldsymbol{\nabla} C_{Na}\right]\right. \\ &- \boldsymbol{u}\left[\frac{C_{Cl}}{m_{Cl}} - \frac{C_{Na}}{m_{Na}}\right] \\ &+ \left.\left[\frac{P_{Cl}}{m_{Cl}} - \frac{P_{Na}}{m_{Na}}\right]\boldsymbol{\nabla}\Phi\right) \quad (28) \end{aligned}$$

According to Equation 23, the following identity is reached:

$$\frac{C_{Cl}}{m_{Cl}} = \frac{C_{Na}}{m_{Na}} \quad (29)$$

Substituting Equation 29 into Equation 28 gives:

$$\begin{aligned} I &= \frac{F}{m_{Cl}}\left(\hat{D}_{Cl} - \hat{D}_{Na}\right)\boldsymbol{\nabla} C_{Cl} \quad (30) \\ &+ F\left(\frac{P_{Cl}}{m_{Cl}} - \frac{P_{Na}}{m_{Na}}\right)\boldsymbol{\nabla}\Phi \quad (31) \end{aligned}$$

Substituting the coefficients defined in Equations 26 into Equation 30, and using Equation 29, the final expression of the current density is obtained:

$$I = \frac{\tau F \phi_l}{m_{Cl}} \left[D_{Cl} - D_{Na} \right] \quad \boldsymbol{\nabla} C$$
$$- \frac{\tau F^2 \phi_l}{RT m_{Cl}} C_{Cl} \left[D_{Cl} + D_{Na} \right] \quad \boldsymbol{\nabla} \Phi \qquad (32)$$

The electric field $\boldsymbol{E} = -\boldsymbol{\nabla}\Phi$ is finally obtained by setting I to zero. If no external electric field is applied, the pore solution is electroneutral everywhere [9]. In the following, the chloride concentration C_{Cl} is denoted by C. The electric field reads:

$$\boldsymbol{E} = -\frac{RT}{FC} \frac{D_{Cl} - D_{Na}}{D_{Cl} + D_{Na}} \boldsymbol{\nabla} C \qquad (33)$$

The electric flux of chloride ions at the macroscale can finally be rewritten as:

$$\boldsymbol{J}_P = P\boldsymbol{E} = \tau \phi_l D_{Cl} \frac{D_{Cl} - D_{Na}}{D_{Cl} + D_{Na}} \boldsymbol{\nabla} C \qquad (34)$$

4.3 Diffusive versus electric flux

Dividing the electric flux (Equation 34) by the diffusive flux (Equation 20), a dimensionless coefficient D_r is obtained:

$$D_r = -\frac{D_{Cl} - D_{Na}}{D_{Cl} + D_{Na}} \qquad (35)$$

The value of D_r is a direct measure of how much the electric field slows down the diffusive flux of chloride ions. Note that it is difficult to separate the two different fluxes in practice, since the diffusive flux induces the electric flux. Therefore, the experimentally obtained effective diffusion coefficients obtained from standard test methods are not pure diffusion coefficients. That is, the effective diffusion coefficient obtained from such methods includes the modification due to the electric flux:

$$D_e^{exp} = \tau D_{Cl} \left(1 + D_r \right) \qquad (36)$$

where D_e^{exp} is the experimentally obtained diffusion coefficient. The coefficient D_r can be derived for more general cases as well, where multiple ion species are present [8]. However, to that end, detailed knowledge of the concentration of each ion species in the pore solution is needed.

4.4 Advective flux

A general expression for the advective flux of chloride ions at the macroscopic scale is:

$$\boldsymbol{J}_A = \boldsymbol{u} C \qquad (37)$$

where $\boldsymbol{J}_A$ is the advective flux and $\boldsymbol{u}$ is the advection velocity obtained by coupling the chloride transport model to a pore solution transport model. The flow of the pore solution is modelled by means of Darcy's law:

$$\boldsymbol{J}_{\phi_l} = -\rho_l \frac{k_l}{\nu_l} \boldsymbol{\nabla} p_l \qquad (38)$$

where $\boldsymbol{J}_{\phi_l}$ is the mass flux of the pore solution ($kg/m^2 s$), ρ_l is the density of the pore solution, k_l is the permeability function (m^2), ν_l the dynamic viscosity of the pore solution ($Pa \cdot s$) and p_l is the pressure of the liquid pore solution. The permeability is the product of the intrinsic permeability coefficient by the permeability function relative to the pore solution:

$$k_l = K k_{rl} \qquad (39)$$

where K is the intrinsic permeability coefficient and k_{rl} the relative permeability function. The capillary pressure is defined as the difference between the pressure of the non-wetting fluid (dry air and water vapour) and the wetting fluid (liquid water):

$$p_c = p_g - p_l \qquad (40)$$

where p_g is the pressure of the gaseous phase and p_l the pressure of the liquid phase. Mainguy et al. [10] observed that, in weakly permeable materials like concrete, there is no significant darcean advective transport of the gaseous phase considered as a whole. Therefore, the gradient of the capillary pressure can be approximated as:

$$\boldsymbol{\nabla} p_c = -\boldsymbol{\nabla} p_l \qquad (41)$$

The mass flux of the pore solution can thus be rewritten as:

$$\boldsymbol{J}_{\phi_l} = \rho_l \frac{k_l}{\nu_l} \boldsymbol{\nabla} p_c \qquad (42)$$

The capillary pressure is a function of the water content ϕ_l, porosity ϕ and temperature T. Equation 42 finally becomes:

$$\boldsymbol{J}_{\phi_l} = \rho_l \frac{k_l}{\nu_l} \left(\frac{\partial p_c}{\partial \phi_l} \boldsymbol{\nabla} \phi_l \; + \; \frac{\partial p_c}{\partial \phi} \boldsymbol{\nabla} \phi + \frac{\partial p_c}{\partial T} \boldsymbol{\nabla} T \right) \tag{43}$$

5 TRANSPORT EQUATIONS

The transport equations are obtained by substituting the previously obtained mass fluxes into the continuity equation.

5.1 Chloride transport

The continuity equation can be expressed as follows:

$$\frac{\partial \varphi}{\partial t} + \boldsymbol{\nabla} . \boldsymbol{J}_{\varphi} = 0 \tag{44}$$

where φ is the conserved quantity and $\boldsymbol{J}_{\varphi}$ is the flux of that quantity. In the case of transport of chloride ions, the bound chloride content needs to be accounted for, which is done by adding a source/sink term:

$$\frac{\partial \varphi}{\partial t} + \boldsymbol{\nabla} . \boldsymbol{J}_{\varphi} = s \tag{45}$$

where s acts as a source if $s > 0$ (bound chlorides dissolve) and as a sink if $s < 0$ (free chlorides are removed due to chloride binding). Generally, the bound chloride concentration depends on the free chloride concentration and on temperature. For the sake of simplicity, the dependence of chloride binding on temperature is ignored in this work. Assuming that the bound chloride concentration C_b solely depends on the free chloride concentration C_f, the chloride transport model reads:

$$\left(1 + \frac{dC_b}{dC_f}\right) \frac{\partial C_f}{\partial t} + \frac{\partial C_p}{\partial t} \boldsymbol{\nabla} . \left(\left[\frac{\boldsymbol{u}}{\phi_l} + \frac{\tau}{\phi_l} D_{Cl} (1 + D_r) \boldsymbol{\nabla} \phi_l \right] C_f \right) = \boldsymbol{\nabla} . \left(\tau D_{Cl} [1 + D_r] \boldsymbol{\nabla} C_f \right) \tag{46}$$

where C_p is the amount of precipitated salt (kg/m^3 of concrete), and $\boldsymbol{u}$ is expressed as:

$$\boldsymbol{u} = \frac{k_l}{\nu_l} \left(\frac{\partial p_c}{\partial \phi_l} \boldsymbol{\nabla} \phi_l + \frac{\partial p_c}{\partial \phi} \boldsymbol{\nabla} \phi + \frac{\partial p_c}{\partial T} \boldsymbol{\nabla} T \right) \tag{47}$$

When chloride ions combine or precipitate, the porosity is reduced and porosity gradients appear, which can be expressed as follows:

$$\boldsymbol{\nabla} \phi = \boldsymbol{\nabla} \phi_0 - \frac{1}{\rho_{fs}} \boldsymbol{\nabla} C_b - \frac{1}{\rho_{ps}} \boldsymbol{\nabla} C_p \tag{48}$$

where ϕ_0 is the initial porosity, while ρ_{fs} and ρ_{ps} are the densities of Friedel's salt and the precipitated salt. Precipitation of salt only occurs when $C > C_{sat}$ where C_{sat} is the saturated concentration. The derivative of C with respect to t is then zero, as well as the gradient of C (no diffusion occurs where salt precipitates). Taking this into account, Equation 46 for areas where chloride precipitation occurs, reads:

$$\frac{\partial C_p}{\partial t} = - \left. \frac{dC_b}{dC_f} \right|_{C_f = \phi_l C_{sat}} C_{sat} \frac{\partial \phi_l}{\partial t} \tag{49}$$

5.2 Pore solution flow

The evolution of the pore solution content is expressed as:

$$\frac{\partial \left(\rho_l \phi_l \right)}{\partial t} = - \boldsymbol{\nabla} . \left(\rho_l \boldsymbol{u} \right) \tag{50}$$

5.3 Heat transfer

The heat transfer is modelled by the linear heat equation with thermal diffusivity α_T (m^2/s):

$$\frac{\partial T}{\partial t} = \boldsymbol{\nabla} . \left(\alpha_T \boldsymbol{\nabla} T \right) \tag{51}$$

6 MATERIAL PARAMETERS

Four different concretes were studied, referred to as *mat1*, *mat2*, *mat3* and *mat4*. The dosages of those materials are listed in Table 1. More details about the materials can be found in [11, 12].

Table 1: Dosages (kg/m^3)

Material	*mat1*	*mat2*	*mat3*	*mat4*
Cement	380	357	380	304
Water	171	194	171	154
Fly ash	0	76	0	0
Silica fume	0	0	0	38
Aggregate	787	770	787	800
Sand	1022	966	1022	1067
Superplasticizer	0.97	0.70	1.30	1.80

6.1 Diffusive material properties

The effective diffusion coefficient D_e (Equation 36), which accounts for both diffusion and the induced migration, must be determined experimentally. The coefficients D_{Cl} and D_r are assumed to depend on temperature according to the Arrhenius equation. The tortuosity-connectivity coefficient is obtained by setting the Hagen-Poiseuille flux of the pore solution in the equivalent pore equal to the Darcy flux [8]. The experimental diffusion coefficient at a given temperature is obtained by fitting the FEM solution of the model to experimental data, namely, the total, free and bound chloride profiles. The total and free concentration profiles were measured according to the standard test methods *UNE-112010:1994* [13] and *RILEM TC 178-TMC* [14]. The sum of the diffusive and induced electric fluxes in function of the experimental diffusion coefficient is:

$$\begin{aligned} \boldsymbol{J}_{DP} &= -D_e^{exp}\left[1-\left(1-\left(\frac{\phi_l}{\phi}\right)^{\frac{1}{e}}\right)^{e}\right]^2 \\ \sqrt{\phi\phi_l} &\ \exp\left(-\frac{E_a}{R}\left[\frac{1}{T}-\frac{1}{T_0}\right]\right)\boldsymbol{\nabla} C \end{aligned} \quad (52)$$

where E_a is the activation energy of the system which depends on the activation energies of the ions in the pore solution [8] (in this case, only Cl^- and Na^+), $T_0 = 20°C$ is the reference temperature at which D_e^{exp} was measured, and e is a material parameter which is determined below.

6.2 Hygroscopic material properties

The hygroscopic properties of the materials were determined by means of absorption-desorption and imbibition tests. In addition, the porosity (accessible to water) was determined by recording the weights of dry and fully saturated concrete samples. The absorption-desorption and imbibition tests were performed according to the standard test methods *UNE-EN ISO 12571* [15] and *ASTM C 1585–04* [16], respectively. The experimental data led to the determination of the capillary pressure (with the capillary hysteresis included), the permeability (K and k_{rl}), as well as the pore size distribution. More details about these procedures can be found in [8]. The following model for the capillary pressure was proposed which fits very well with the experimental data [8]:

$$\begin{aligned} p_c &= A(T)\left(atan\left(a\left[b-\phi_l\right]\right)\right. \\ &+ \left. atan\left(a\left[\phi-b\right]\right)\right) \end{aligned} \quad (53)$$

where $A(T)$ is the capillary modulus which depends on temperature in the same way as the surface tension of water does, and a and b are parameters which depend on the microstructure of the materials. The relative permeability k_{rl} was modelled by means of the well known van Genuchten model [17]:

$$k_{rl} = \sqrt{\frac{\phi_l}{\phi}}\left[1-\left(1-\left(\frac{\phi_l}{\phi}\right)^{\frac{1}{e}}\right)^{e}\right]^2 \quad (54)$$

The constants a, b and e, as well as the intrinsic permeability coefficient K were determined by fitting the FEM solution to the experimental data.

6.3 Results

From the experimentally obtained free and total chloride concentrations, the bound chloride content was obtained by calculating the difference between the total and the free chloride contents. A good relation was found between the bound and the free chloride concentrations by means of the Langmuir model:

$$C_b(C_f) = \tilde{C}_b\frac{KC_f}{1+KC_f} \quad (55)$$

where $\tilde{C}_b$ is the maximum bound concentration and K is the equilibrium constant.

The samples were submerged in a *NaCl* solution of $0.5M$ for 546 days. The effective diffusion coefficient D_e^{exp} was found by fitting the FEM solution to the experimental data. The results are shown in figure 2. The fitting analysis showed very good results for all the materials except for *mat3*. This is explained below. The contents of Al_2O_3 (responsible for the chemical choride binding) and the contents of SiO_2 (responsible for the *C-S-H* which retains chlorides physically) for each material are listed in Table 2.

Table 2: Aluminates and silicates (kg/m^3)

Material	*mat1*	*mat2*	*mat3*	*mat4*
Al_2O_3	13.1480	35.3042	28.1200	10.5184
SiO_2	11.6280	41.7498	101.46	41.6024

The SiO_2 content of material *mat3* is significantly higher than for the other materials. Furthermore, its content of aluminates is almost as important as for material *mat2*. This leads us to believe that the binding capacity of material *mat3* is at least as important as that of material *mat2*. Luo et al. [18] found that cement with slag increases the chemical binding capacity of concrete. Glasser et al. [19] reported such increase of the physical binding onto the hydrate slag walls which present a high specific surface. This, however, contradicts the experimental data. The experimental method for determining the free chloride concentration plausibly detected an important part of the physically adsorbed chlorides as free chloride ions and, therefore, underestimated the bound chloride content. As can be observed in figure 2, the free chloride content of material *mat3* reaches values higher than $3kg/m^3$. The porosity of material *mat3* was determined to be $\phi = 0.125$ and the free chloride concentration of the solution was 0.5M ($C = 18.5g/l$). The free chloride concentration C near the surface, according to the experimental data, would be greater than $3 \times 12.5\% = 24g/l$ which is impossible.

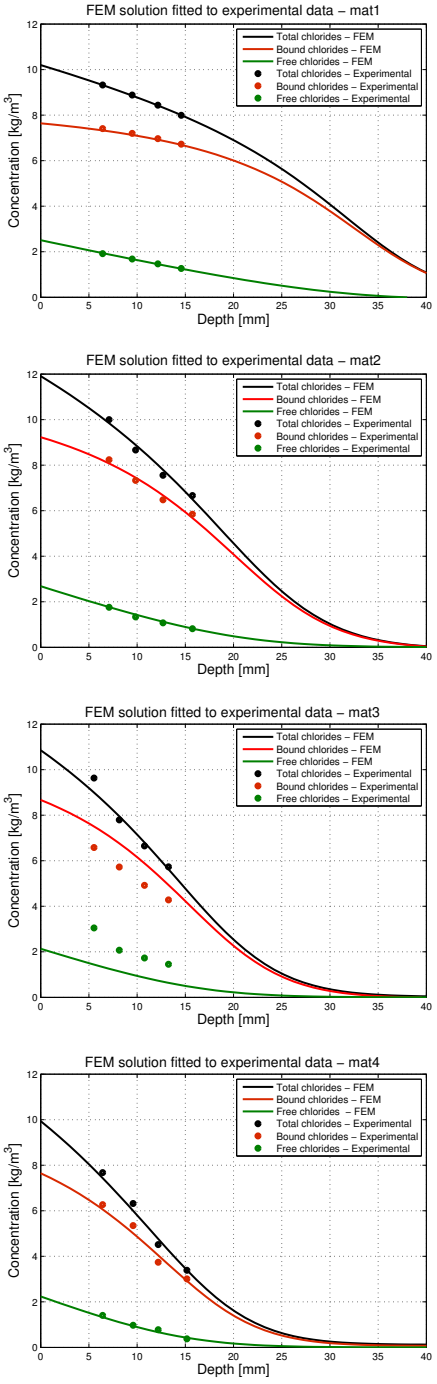

Figure 2: Total, free and bound chloride concentrations for materials *mat1-mat4*.

Finally, the Langmuir model of material *mat2* was used to model the bound chloride content of *mat3*, with good results. In figure 2, it may be observed that the model seems to

fit very well to the total chloride profile. The obtained diffusion coefficients, as well as the overall porosities, are listed in Table 3.

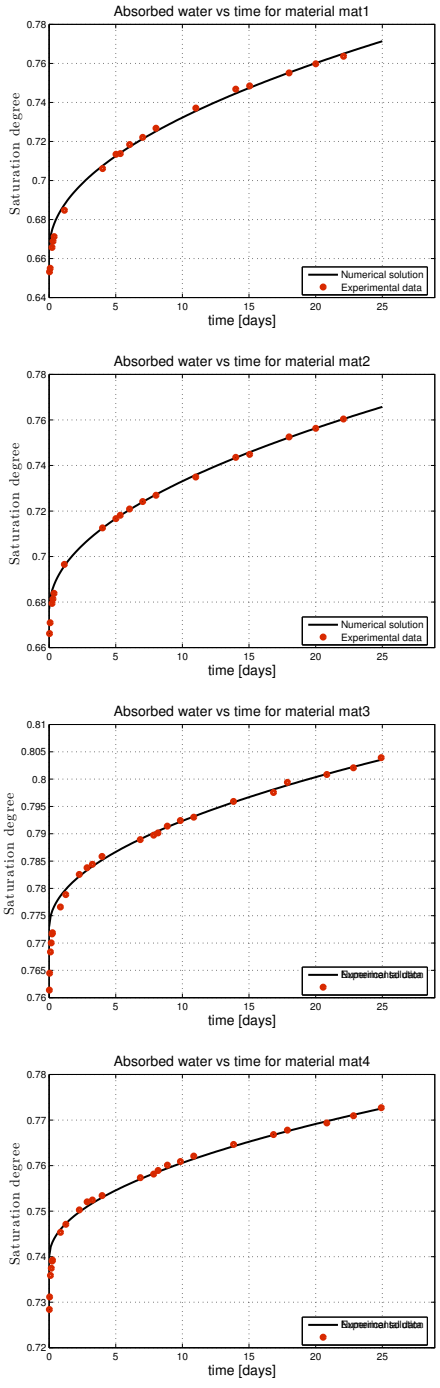

Figure 3: Imbibition test for materials *mat1-mat4*.

Fitting the FEM solution to the experimental data obtained from the imbibition tests allowed calculation of the intrinsic permeability coefficient K for each material. The results are plotted in figure 3. The capillary pressure model (Equation 53) was fitted to experimental data and is plotted in figure 4. The intrinsic permeability coefficients are given in Table 3.

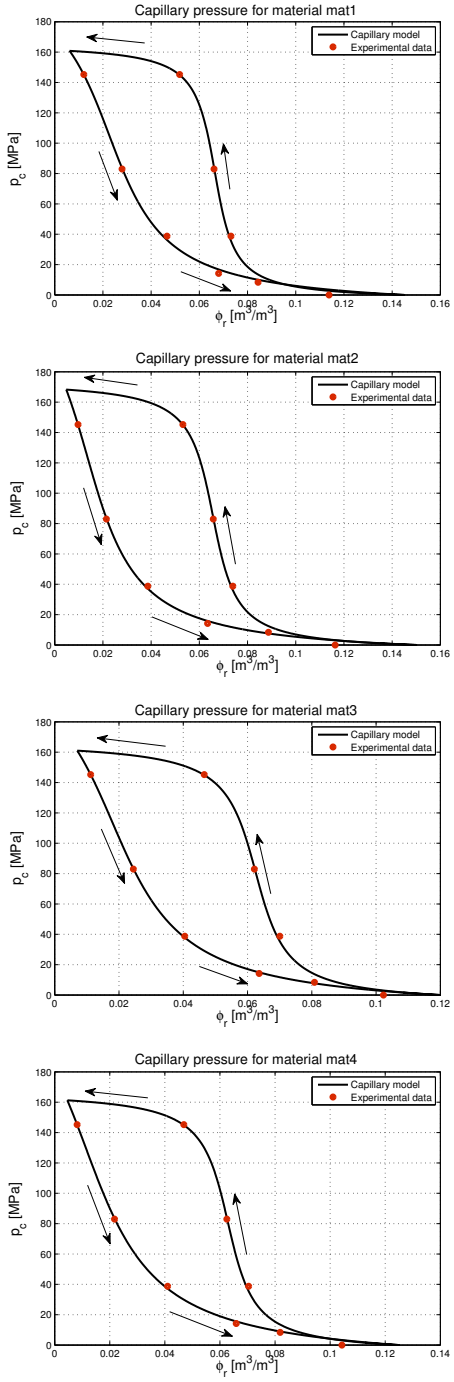

Figure 4: Capillary pressure for materials *mat1-mat4*.

Table 3: Porosity (%), diffusion coefficient $\times 10^{-11} m^2/s$ and permeability coefficient $\times 10^{-21} m^2$

Material	*mat1*	*mat2*	*mat3*	*mat4*
ϕ	14.5	15.0	12.0	12.5
D_e^{exp}	4.5	2.5	2.0	1.2
K	2.70	2.45	0.27	0.20

7 FEM SOLUTION

The pore solution flow and heat transfer models were solved by means of the classical Galerkin formulation. The chloride transport model was modelled by means of the streamline upwind Petrov-Galerkin (SUPG) method. The classical Galerking formulation would give unstable results when advection predominates over diffusion. The model was implemented for linear and quadratic elements on a *1D*-mesh, as well as on a *2D*-mesh of triangular elements. More details on the modelling can be found in [8]. An example of unstable results is shown in figure 5. A fully saturated concrete sample, with a uniformally distributed chloride concentration of $5g/l$, is dried during 5 days at a temperature of $20°C$ and relative humidity 80%.

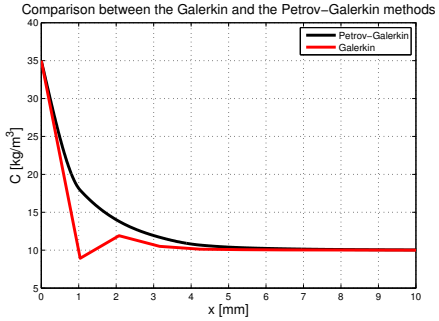

Figure 5: Galerking vs. Petrov-Galerking solutions.

In order to illustrate the capabilities of the model, the following simulation is considered. A concrete sample is initially saturated with water. An aqueous solution of $C = 100g/l$ is imposed on one side of the sample for 125 days. During that time, the only transport mechanism considered is diffusion (and the induced electric flux). The numerical experiment was performed by imposing different relative humidities on the same side of the sample for 55 days, so that the sample underwent a drying process. The relative humidities are chosen to be $h_r = 70\%$, 50% and 30% at a temperature of $20°C$. The results are plotted in figures 6-9.

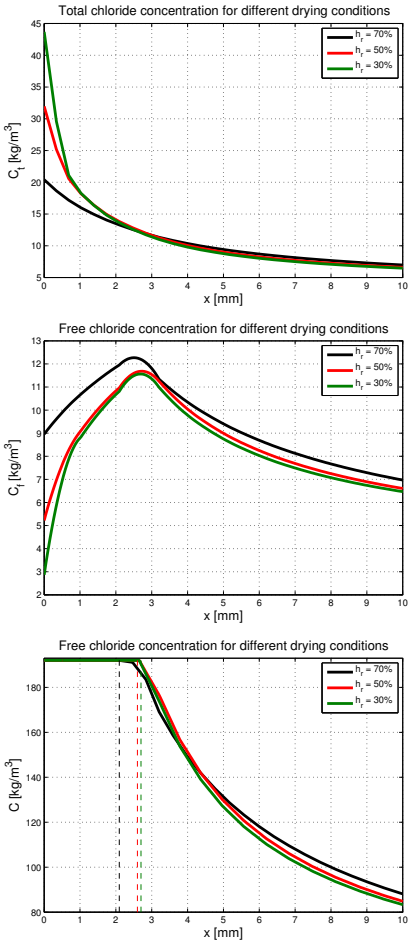

Figure 6: Concentration profiles C_t (top), C_f (middle) and C (bottom).

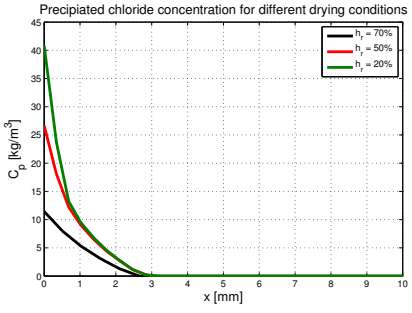

Figure 7: Precipitated chlorides C_p.

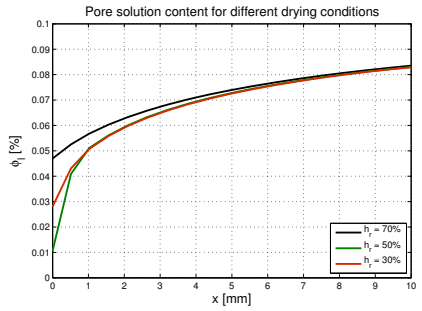

Figure 8: Pore water content ϕ_l.

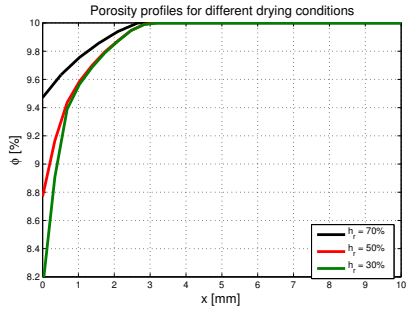

Figure 9: Porosity ϕ.

8 CONCLUSIONS

The transport equations of chloride ions in hardened concrete at the macroscopic scale were derived from the transport equations at the microscopic scales. This was performed by defining an equivalent pore which accounts for that part of the porous network filled with pore solution. The advective mass flux was modelled by means of Darcy's law. The material properties were determined by fitting the numerical solution to experimental data obtained through standard test methods. Finally, the chloride transport equation, pore solution transport equation, as well as the heat transfer equation were solved simultaneously by means of the FEM method.

9 ACKNOWLEDGEMENTS

The authors gratefully acknowledge the financial support for the research provided by the Spanish Ministerio de Ciencia e Innovación under grants IPT-42000-2010-31 and DPI2011-24876.

REFERENCES

[1] C.L. Page, N.R. Short, and A. El Tarras. Diffusion of chloride ions in hardened cement pastes. *Cement and Concrete Research*, 11(3):395 – 406, 1981.

[2] S. Goto and D.M. Roy. Diffusion of ions through hardened cement pastes. *Cement and Concrete Research*, 11(5-6):751 – 757, 1981.

[3] A.V. Saetta, R.V. Scotta, and R.V. Vitaliani. Analysis of chloride diffusion into partially saturated concrete. *Materials Journal*, 90(5):441 – 451, 1993.

[4] O. Coussy and F.J. Ulm. Elements of durability mechanics of concrete structures. In F.J. Ulm, Z.P. Bažant, and F.H. Wittmann, editors, *Creep, Shrinkage and Durability Mechanics of Concrete and other Quasi-Brittle Materials*, pages 393–409. Elsevier, Oxford, United Kingdom, 2001.

[5] E. Samson, J. Marchand, and J.J. Beaudoin. Describing ion diffusion mechanisms in cement-based materials using the homogenization technique. *Cement and Concrete Research*, 29(8):1341 – 1345, 1999.

[6] E. Samson, G. Lemaire, J. Marchand, and J.J. Beaudoin. Modeling chemical activity effects in strong ionic solutions. *Computational Materials Science*, 15(3):285 – 294, 1999.

[7] E. Samson and J. Marchand. Numerical solution of the extended nernst-planck model. *Journal of Colloid and Interface Science*, 215(1):1 – 8, 1999.

[8] M. Fenaux. *Modelling of chloride transport in non-saturated concrete. From Microscale to Macroscale*. PhD thesis, Escuela Técnica Superior de Ingenieros de Caminos, Canales y Puertos, Madrid, Spain, 2012.

[9] J.O'M. Bockris, A.K.N. Reddy, and M.E. Gamboa-Aldeco. *Modern Electrochemistry 2A: Fundamentals of Electrodics*. Springer, 2 edition, January 2001.

[10] M. Mainguy, O. Coussy, and V. Baroghel-Bouny. Role of air pressure in drying of weakly permeable materials. *Journal of Engineering Mechanics*, 127(6):582–592, 2001.

[11] S. Mahmoud Abdelkader. *Influencia de la composición de distintos hormigones en los mecanismos de transporte de iones agresivos procedentes de medios marinos*. PhD thesis, Escuela Técnica Superior de Ingenieros de Caminos, Canales y Puertos, Madrid, Spain, June 2010.

[12] S. Mahmoud Abdelkader, E. Reyes Pozo, and A. Moragues Terrades. Evolution of microstructure and mechanical behavior of concretes utilized in marine environments. *Materials & Design*, 31(7):3412 – 3418, 2010.

[13] *UNE 112010, Corrosión de armaduras. Determinación de cloruros en hormigones endurecidos y puesto en servicio.* AENOR, 2011.

[14] M. Castellote and C. Andrade. TC 178-TMC: Testing and modelling chloride penetration in concrete. Round-Robin test on chloride analysis in conrete – Part II: Analysis of water soluble chloride content. *Materials and Structures*, 34(244):589–598, 2001.

[15] *UNE-EN ISO 12571, Prestaciones higrotérmicas de los productos y materiales para edificios*. AENOR, 2000.

[16] *ASTM C 1585-04, Standard test method for measurement of rate of absorption of water by hydraulic-cement concretes*, West Conshohocken, PA, United States, 2008. ASTM International.

[17] M.Th. van Genuchten. A closed-form equation for prediciting the hydraulic conductivity of unsaturated soils. *Soil Science Society of America*, 44:892–898, 1980.

[18] Rui Luo, Yuebo Cai, Changyi Wang, and Xiaoming Huang. Study of chloride binding and diffusion in ggbs concrete. *Cement and Concrete Research*, 33(1):1 – 7, 2003.

[19] F.P. Glasser, J. Marchand, and E. Samson. Durability of concrete – degradation phenomena involving detrimental chemical reactions. *Cement and Concrete Research*, 38(2):226 – 246, 2008.